Similarity and dissimilarity between water and methanol in solvent effects on the spectroscopic properties of aniline: Molecular dynamics and time-dependent DFT studies

Watanabe, Takumi
Department of Chemistry, Graduate School of Science, Kyushu University

Ohashi, Kazuhiko
Department of Chemistry, Faculty of Science, Kyushu University

出版情報：Computational and Theoretical Chemistry. 1215, pp.113850-, 2022-09. Elsevier
バージョン：
権利関係：

Similarity and dissimilarity between water and methanol in solvent effects on the spectroscopic properties of aniline: Molecular dynamics and time-dependent DFT studies

Takumi Watanabe [a], Kazuhiko Ohashi [b,*]

[a] *Department of Chemistry, Graduate School of Science, Kyushu University, Motooka, Fukuoka 819-0395, Japan*

[b] *Department of Chemistry, Faculty of Science, Kyushu University, Motooka, Fukuoka 819-0395, Japan*

ABSTRACT

Solvent effects on the absorption spectra of aniline ($C_6H_5NH_2$) are investigated. DFT and TD-DFT calculations for 1:1 aniline–water and aniline–methanol complexes predict that an N-bound isomer with an OH···N bond is the global minimum in the S_0 state, while an H-bound isomer with an NH···O bond becomes lower in the S_1 state. The N-bound and H-bound solvents cause blue and red shifts, respectively. MD simulations are used to allocate solvent molecules around aniline for constructing model structures with a complete solvation shell. TD-DFT calculations for the model structures are successful in reproducing the experimental observation that the absorption band in methanol is less blue-shifted than that in the water. At least one water molecule is incessantly bound to the nitrogen atom and causes the significant blue shift. In contrast, methanol molecules are less frequently bound to the nitrogen atom and therefore the blue-shifting effect is less significant.

Keywords:

aniline; hydroxylic solvents; absorption spectra; solvent effects; molecular dynamics simulations; time-dependent density functional theory

* Corresponding author.

E-mail address: kazu@chem.kyushu-univ.jp (K. Ohashi).

1. Introduction

Gas-phase clusters consisting of a solute and a few numbers of solvent molecules have been considered as microscopic models for the solute surrounded by solvent molecules in condensed phases [1–3]. Environmental effects on the properties of the solute have been modeled by successive addition of single solvent molecules to the previous-sized cluster. Although a variety of solute–solvent combinations have been studied, much attention has been focused on aromatic solute–(protic solvent)$_n$ clusters, with special emphasis on the clusters involving intermolecular hydrogen bond(s) [1–3].

For many aromatic–(solvent)$_n$ clusters, electronic spectra have been recorded and the origin transitions have been identified clearly. The direction and magnitude of the electronic frequency shift can be used as a qualitative probe of the mode of binding of the solvent molecule(s) to the aromatic [1]. For phenol–$(H_2O)_n$ clusters, the strongest binding site in phenol is the OH group, although waters also interact with the π electrons of the aromatic ring. The origin band of phenol–$(H_2O)_1$ is red-shifted by hundreds of wavenumbers from that of the bare phenol. Such a red shift is a signature that the aromatic OH group donates the hydrogen atom to surrounding solvent molecule(s). In phenol–$(H_2O)_2$ and phenol–$(H_2O)_3$, the water molecules and the OH group of phenol form hydrogen-bonded rings, where the oxygen atom of phenol accepts a hydrogen atom from one of the additional waters. As a result, the origins of these clusters are shifted back toward the bare-phenol origin from that of phenol–$(H_2O)_1$. The red- or blue-shift of the $S_1 \leftarrow S_0$ origin band relative to the bare phenol gives valuable hints on the hydrogen bonding between phenol and the water moiety [1,2].

Gas-phase cluster studies have only rarely achieved the ideal of forming a complete solvation shell around a solute. A full solvation shell has been achieved in some cases of ionic clusters, but in neutral clusters, the solvent molecules are hydrogen bonded to one another about the strongest binding site(s) of the solute [1]. Phenol–$(H_2O)_n$ clusters with $n \leq \approx 50$ have been considered to adopt essentially the same network structures as $(H_2O)_{n+1}$ clusters, where the phenol molecule attaches to the surface of the $(H_2O)_n$ clusters and inserts the OH group into the hydrogen bond network of the waters [4,5]. Similarly, benzene–

$(H_2O)_n$ clusters have structures in which benzene is bonded to the surface of the $(H_2O)_n$ cluster [1]. Thus, water molecules rarely form a complete solvation shell around an aromatic solute in gas-phase clusters. It can be said that this is a shortcoming of the use of gas-phase clusters for modeling the solvation of neutral solute molecules.

In contrast to accumulated knowledge about the phenol–$(H_2O)_n$ clusters [1–5], aniline–$(H_2O)_n$ clusters have been highly elusive [6]. Nakanaga et al. calculated three isomeric structures of aniline–$(H_2O)_1$ in the S_0 state [7]. The first one contains a hydrogen bond between the NH group of aniline and the oxygen atom of water (H-bound isomer). The second has a hydrogen bond between the OH group of water and the nitrogen atom of aniline (N-bound isomer). The third has hydrogen bonds between the OH groups of water and the π electrons of the aromatic ring (π-bound isomer). The N-bound isomer was predicted to be most stable from calculations at the MP2/6-31G(d,p) level [7]. Such an N-bound isomer was confirmed by a microwave spectroscopic study [8]. Piani et al. recorded an electronic spectrum of aniline–$(H_2O)_1$, which shows only broad absorption with no noticeable origin transition [9]. Piani et al. predicted the N-bound isomer to become significantly less stable in the S_1 state from calculations at the CIS and CASSCF levels [9]. The absence of a prominent origin transition might be caused by large changes in the geometry of the complex on the electronic excitation. In an electronic spectrum of aniline–$(H_2O)_1$, León et al. found a sharp band at ≈900 cm^{-1} to the blue of the origin of aniline [6]. They performed calculations for the three isomers at the M06-2X/6-311++G(d,p) level and confirmed that the N-bound isomer is lowest in energy. León et al. also succeeded in recording an infrared spectrum of aniline–$(H_2O)_1$ through an infrared/ultraviolet double resonance technique; the spectrum was consistent with the N-bound isomer [6].

Much the same is true for the aniline–$(CH_3OH)_1$ complex. A microwave spectroscopic study concluded an N-bound isomer, with the methyl group of methanol directing to the phenyl ring [10]. Electronic spectra show only broad absorption with no noticeable origin transition [9,11]. Theoretical calculations predicted the N-bound isomer to be more stable than an H-bound isomer [12]. Aniline–$(CH_3OH)_{1–5}$ clusters were also

calculated [13], where aniline is attached to the $(CH_3OH)_n$ clusters, as in the case of phenol–$(H_2O)_n$.

For aniline dissolved in solutions, the maximum of the $S_1 \leftarrow S_0$ absorption band in water was observed to be blue shifted from that in cyclohexane [14]. Because analogous shift was observed for *N*,*N*-dimethylaniline, it was suggested that the spectral shift was caused by hydrogen bonding between the OH group of water and the nitrogen atom of aniline [14,15]. The blue shifts of the $S_1 \leftarrow S_0$ band in hydroxylic solvents were also reported in subsequent studies [16,17]. Since the dipole moment of aniline was shown to increase on the $S_1 \leftarrow S_0$ excitation, Köhler considered that the O–H···N hydrogen bond should become weaker, while the N–H···O hydrogen bond should be stabilized in the S_1 state [17].

We intend to carry out theoretical investigations on the $S_1 \leftarrow S_0$ transition of aniline in solutions. If we add solvent molecules one by one to aniline, then it would require incredibly large numbers of steps to achieve a complete solvation shell. Instead, we use molecular dynamics (MD) simulations to allocate the solvent molecules around aniline all at once. With the resulting model structures for aniline in water and methanol solutions, the $S_1 \leftarrow S_0$ absorption spectra are simulated from time-dependent density functional theory (TD-DFT) calculations. A combination of MD simulations and TD-DFT calculations has been widely used for modeling absorption spectra of molecules in solutions [18–21]. The technique is suitable for our purpose and employed in the present work. The theoretical results are compared with the experimental spectra for validating the reliability of the model structures. Then we explore the site dependence of the solvent effects on the $S_1 \leftarrow S_0$ transition of aniline, by analyzing sub-clusters extracted from the central region of the model structures. As we all know, both water and methanol are polar and protic solvents. Nevertheless, we have found a noticeable difference in the solvent effects between water and methanol.

2. Methods

Quantum chemistry calculations are carried out with the Gaussian 16 package [22].

DFT and TD-DFT methods are employed by using the M06-2X variant of hybrid Minnesota functionals. Dispersion interaction is corrected by addition of the D3 version of Grimme's dispersion with the original D3 damping function (GD3). The 6-311++G(d,p) basis set is used unless otherwise stated. The level of theory is referred to as M06-2X(GD3)/6-311++G(d,p). Self-consistent reaction field method with polarizable continuum model (PCM) is incorporated to implicitly account for solvents surrounding the solute and the explicit solvents. Geometries of 1:1 aniline–solvent complexes in the S_0 and S_1 states are optimized from DFT and TD-DFT calculations, respectively, without any symmetry constraints. For both of the optimized geometries, harmonic vibrational frequencies are evaluated to confirm the absence of imaginary-frequency vibration. Energies of the S_0 and S_1 states are reported after zero-point-energy (ZPE) correction. The $S_1 \leftarrow S_0$ transition energies are evaluated from TD-DFT method. All the values calculated for the transition energies are scaled with a factor of 0.9232 for a direct comparison with the experimental data, as described in section A.1 of Supplementary material (SM).

MD simulations are carried out using the Amber 18 package [23]. First, the electrostatic potential is obtained for aniline from DFT calculations; atom-centered partial charges are evaluated with the restrained electrostatic potential (RESP) approach. Aniline is solvated in a cubic box with the side length of 30 Å and the periodic boundary conditions are imposed. Water is described using the TIP3P model. The generalized Amber force field (GAFF) is used. The amber ff14sb force field is used for methanol solvation. After energy minimization, the equilibration trajectory is run in the NPT ensemble (1.0 bar, 300 K). The pressure and temperature are kept constant using the Berendsen algorithm. During the simulations, the internal coordinates of aniline are fixed. The SHAKE method is employed to constrain the lengths of bonds involving hydrogen atoms. Long range electrostatic interactions are computed by the Particle Mesh Ewald method.

3. Results and discussion

3.1. Experimental absorption spectra

Fig. 1 shows ultraviolet absorption spectra of aniline dissolved in cyclohexane (c-C_6H_{12}), methanol (CH_3OH), and water (H_2O). The maximum of the band is located around 34800, 35150, and 35700 cm^{-1} for the spectra in cyclohexane, methanol, and water, respectively. The maximum absorbance of the spectra in methanol and water is smaller than that in cyclohexane by a factor of approximately 0.8. The spectrum in cyclohexane shows vibrational structures, while the other spectra are structureless. These results are consistent with the ones reported previously [14–17]. The absorption is assigned to the $S_1 \leftarrow S_0$ transition. This transition has been referred to as an $n\pi^*$ transition in several solution-phase studies, probably because the absorption band shows a blue shift in polar solvents. However, natural transition orbitals (Fig. S1b of SM) indicate that the $S_1 \leftarrow S_0$ transition bears a $\pi\pi^*$ character in addition to the $n\pi^*$ character, as demonstrated in section A.1 of SM.

The main subject of this work is to acquire information on the details of the aniline–solvent interactions from theoretical calculations. To this end, it is necessary to prepare model structures of aniline surrounded by solvent molecules. The requirement is that characteristic features of the absorption spectra can be reproduced with the model structures.

3.2. Continuum solvation model

In a first step, an aniline molecule is placed in a cavity within the solvent reaction field. We use the integral equation formalism variant of polarizable continuum model (IEFPCM). For reference, the values of the dielectric constant are as follows: 2.0165 for cyclohexane, 32.613 for methanol, and 78.3553 for water [22].

3.2.1 Geometries and electronic properties of aniline

Information of aniline in vacuum is described in section A.1 of SM. Here, the geometries of aniline in the S_0 and S_1 states are optimized in each solvent at the M06-2X(GD3)/6-311++G(d,p) level. Table S1 of SM collects the values calculated for the inclination angle of the NH_2 group (θ), the electric dipole moment (μ), and the polarizability volume (α). The values of θ are approximately 41° in the S_0 state, but they approach 0° in

the S_1 state. Both the μ and α values of the S_0 state and the μ values of the S_1 state increase with increasing the dielectric constant of the solvent. Exceptionally, in the S_1 state, the α value in cyclohexane is largest.

3.2.2 $S_1 \leftarrow S_0$ transition

Table S2 of SM lists the energies for the $S_1 \leftarrow S_0$ transition. The 0–0 transition energy ($h\nu_{0\text{–}0}$) is the difference between the zero-point energy levels of the S_1 and S_0 states. The vertical transition energy ($h\nu_{\text{vert}}$) is that required for the transition from the minimum of the S_0 state to the point on the S_1 potential energy surface that is at the same geometry as the S_0 state. As shown in Table S1 of SM, both the μ and α values in vacuum increase on the $S_1 \leftarrow S_0$ transition. Accordingly, the S_1 state is expected to be more stabilized than the S_0 state in the polarizable continuum. In fact, the $h\nu_{0\text{–}0}$ values in the solvent are smaller than that in vacuum and decrease with increasing the dielectric constant of the solvent. The $h\nu_{\text{vert}}$ values show a similar solvent dependence. In contrast, the energy corresponding to the observed absorption maximum is smallest in cyclohexane and increases with increasing the dielectric constant. The discrepancy suggests that the continuum solvation model is not adequate for describing the solvent effect on the $S_1 \leftarrow S_0$ spectra of aniline. This seems reasonable because the $S_1 \leftarrow S_0$ transition bears the $n\pi^*$ character in part; the non-bonding (n) orbital on the nitrogen atom of aniline tends to be stabilized substantially by hydrogen-bonding interaction with a solvent molecule.

The $S_1 \leftarrow S_0$ spectra of aniline and other substituted benzenes are known to exhibit rich vibronic structures [24]. For aniline, the spectra in hydrocarbon solutions exhibit some vibrational structures [15], as shown in Fig. 1 for the cyclohexane solution. Then we carry out calculations of the vibronic spectra; the details are described in section A.2 of SM. The vibrational structures of the experimental spectrum in cyclohexane are satisfactorily reproduced when the theoretical line spectra are convoluted with a width of 175 cm^{-1}, as demonstrated in Fig. S2 of SM. Fig. 2 displays the vibronic spectra of aniline in three solvents convoluted with this width. The theoretical spectra of the water and methanol

solutions also exhibit vibrational structures. However, the corresponding experimental spectra are structureless as shown in Fig. 1. The reason for the disappearance of the vibrational structures in the experimental spectra of the water and methanol solutions will be discussed in section 3.3.4.

3.3. Aniline with one explicit solvent

In a second step, we consider a complex consisting of an aniline (abbreviated to An) and a single solvent molecule. Such a 1:1 aniline–solvent complex has been targets of numbers of experimental and theoretical studies using gas-phase clusters [3,6–13]. For a comparison purpose, we perform DFT calculations for the complexes in vacuum; the results are described in section A.3 of SM. Here, such complexes are placed in the polarizable continuum. The labels attached to the complexes in vacuum (Figs. S6–8 of SM) are also used here, because the optimized geometries in the polarizable continuum are quite similar to those in vacuum. We study the complexes with cyclohexane in addition to water and methanol, because it is helpful to compare the solvent effects on the transition energy between solvents with and without hydrogen-bonding ability.

3.3.1 An(H_2O)$_1$

As in the case in vacuum, the three isomers are considered for An(H_2O)$_1$ in the polarizable continuum: N-bound, H-bound, and π-bound isomers. Fig. 3a–c illustrates the optimized geometries of the three isomers in the S_0 state. The dissociation energies are tabulated in Table S3 of SM. In the N-bound isomer W0-N (Fig. 3a), the O–H···N angle is 170° and the H···N distance is 1.95 Å. In the H-bound isomer W0-H (Fig. 3b), the N–H···O angle is 167° and the H···O distance is 2.02 Å. In the π-bound isomer W0-π (Fig. 3c), the two OH groups of water point to the C3 and C6 atoms; the distance between the O atom and the center of the phenyl ring ($R_{O–CM}$) is 3.15 Å. The W0-Hπ isomer (Fig. S6b of SM) found in vacuum is not stable in the polarizable continuum. W0-N is lowest in energy; W0-H and W0-π lie 6.3 and 3.7 kJ mol^{-1} above W0-N, respectively. The energy ordering is the same as

that in vacuum, but the energy differences become larger than those in vacuum.

The S_0 structure is taken as an initial geometry and the subsequent optimization is carried out in the S_1 state. Fig. 3d,e depicts the optimized geometries of the H-bound isomer W1-H (Fig. 3d) from W0-H and the π-bound isomer W1-π (Fig. 3e) from W0-π. In both isomers, the phenyl ring undergoes out-of-plane distortion in the S_1 state, as described for the bare aniline in section A.1 of SM. For the H-bound isomer, the S_1 optimization reduces the θ value from 40° to 0.5° while maintaining the N–H···O hydrogen bond. The N–H···O angle is 170° and the H···O distance is 1.87 Å. The $S_1 \leftarrow S_0$ excitation shortens the H···O distance by 0.15 Å and increases the dissociation energy from 9.9 to 16.0 kJ mol^{-1}. For the π-bound isomer, the $S_1 \leftarrow S_0$ excitation shortens the R_{O-CM} distance by 0.13 Å and increases the dissociation energy from 12.6 to 16.6 kJ mol^{-1}. For the N-bound isomer, on the other hand, the S_1 optimization starting from W0-N evolves smoothly to a π-bound isomer. As in the case in vacuum, all attempts with other initial geometries fail to find a potential-energy minimum corresponding to the N-bound isomer in the S_1 state.

3.3.2 An(CH$_3$OH)$_1$

As in the case of An(H$_2$O)$_1$, the three isomers are considered for An(CH$_3$OH)$_1$. Fig. 3f–h exhibits the optimized geometries of the three isomers in the S_0 state. In the N-bound isomer M0-N (Fig. 3f), the O–H···N angle is 167° and the H···N distance is 1.98 Å. In the H-bound isomer M0-H (Fig. 3g), the N–H···O angle is 159° and the H···O distance is 2.01 Å. In the π-bound isomer M0-π (Fig. 3h), the OH group of methanol points to the C3 atom. M0-N is lowest in energy; M0-H and M0-π lie 7.2 and 5.2 kJ mol^{-1} above M0-N, respectively. The energy differences among the isomers become larger than those in vacuum.

Fig. 3i,j shows the optimized geometries of the H-bound isomer M1-H (Fig. 3i) from M0-H and the π-bound isomer M1-π (Fig. 3j) from M0-π. For the H-bound isomer, the S_1 optimization reduces the θ value from 41° to 3.3° while maintaining the N–H···O hydrogen bond. The N–H···O angle is 160° and the H···O distance is 1.84 Å. The $S_1 \leftarrow S_0$ excitation

shortens the H···O distance by 0.17 Å and increases the dissociation energy from 16.5 to 22.3 kJ mol^{-1}. For the π-bound isomer, the methanol molecule undergoes reorientation until the OH group points to the C2 atom in M1-π. The $S_1 \leftarrow S_0$ excitation increases the dissociation energy from 18.5 to 22.5 kJ mol^{-1}. Meanwhile, the convergence is not achieved during the S_1 optimization starting from M0-N. Manual adjustment of the geometries arrives at M1-N (not shown), in which the O–H···N angle is 163° and the H···N distance is 2.33 Å. The $S_1 \leftarrow S_0$ excitation decreases the dissociation energy from 23.7 to 12.2 kJ mol^{-1}.

3.3.3 An(c-C_6H_{12})$_1$

We examine the four isomers, which are considered for An(c-C_6H_{12})$_1$ in vacuum in section A.3.3 of SM. In cH0-I (cf. Fig. S8b of SM) with cyclohexane on top of aniline, the distance between the center-of-masses of the two molecules ($R_{CM–CM}$) is 3.92 Å and the dissociation energy is 21.7 kJ mol^{-1}. In cH0-II (cf. Fig. S8c of SM), where the cyclohexane ring is inclined with respect to the aniline ring, the $R_{CM–CM}$ distance is 4.12 Å. In cH0-III and cH0-IV (cf. Fig. S8d,e of SM), cyclohexane is located on the side of aniline in a T-shaped configuration; cyclohexane is close to the C3 and C4 atoms of aniline in cH0-III, while to the C2 and C3 atoms in cH0-IV. The $R_{CM–CM}$ distances are 5.71 and 5.33 Å in cH0-III and cH0-IV, respectively. cH0-I is lowest in energy; cH0-II, cH0-III, and cH0-IV lie 1.7, 13.2, and 13.0 kJ mol^{-1} above cH0-I, respectively. The energy differences among the isomers are comparable with those in vacuum.

For each isomer, the S_1 optimization starting from the S_0 minimum reduces the θ value from ≈41° to less than 5° while maintaining the mutual orientation of the two moieties. The $S_1 \leftarrow S_0$ excitation decreases the dissociation energies of cH0-I and cH0-II by 2.3 and 1.3 kJ mol^{-1}, respectively, as listed in Table S3 of SM. The excitation decreases the dissociation energy of cH0-III while increases that of cH0-IV, but the changes in energy are at most 0.5 kJ mol^{-1}.

3.3.4 $S_1 \leftarrow S_0$ transition

As described in section 3.3.3, the $S_1 \leftarrow S_0$ excitation only slightly affects the intermolecular interaction in An(c-C_6H_{12})$_1$. Meanwhile, the $S_1 \leftarrow S_0$ excitation strengthens the interactions in the H-bound and π-bound isomers of An(H_2O)$_1$ and An(CH_3OH)$_1$, whereas weakens the interactions in the N-bound isomer of An(CH_3OH)$_1$ and presumably of An(H_2O)$_1$, as described in sections 3.3.1 and 3.3.2. Table S4 of SM collects the energies calculated for the 0–0 transition ($h\nu_{0-0}$) and the vertical transition ($h\nu_{vert}$) for the respective isomers along with the bare aniline. Fig. 4 represents stick diagrams of $h\nu_{0-0}$ and $h\nu_{vert}$. For both An(H_2O)$_1$ and An(CH_3OH)$_1$, the 0–0 transitions of the H-bound and π-bound isomers show red shifts from that of the bare aniline. On the other hand, the 0–0 transition of the N-bound isomer of An(CH_3OH)$_1$ exhibits a blue shift. The $h\nu_{0-0}$ value is not available for the N-bound isomer of An(H_2O)$_1$, because no potential-energy minimum is found in the S_1 state. The vertical transitions of the H-bound and π-bound isomers also show red shifts, whereas those of the N-bound isomers exhibit blue shifts. The vertical transition of the N-bound isomer of An(H_2O)$_1$ is predicted 248 cm^{-1} to the blue of that of An(CH_3OH)$_1$. The relative location is consistent with that of the absorption maximum of the experimental spectra. This may imply that at least one explicit solvent, particularly binding to the nitrogen atom of aniline, is necessary to reproduce the solvent effect on the absorption spectra.

Let us look at the variations in the vertical transition energies among the isomers. For An(c-C_6H_{12})$_1$, the differences among the four isomers are at most 137 cm^{-1}. For An(H_2O)$_1$ and An(CH_3OH)$_1$, on the other hand, the differences among the three isomers amount to 1776 and 1422 cm^{-1}, respectively. This means that the transition energies of An(c-C_6H_{12})$_1$ are insensitive to the location of the solvent. Therefore, inhomogeneous broadening should be insignificant for the spectrum of the cyclohexane solution. Meanwhile, the transition energies sensitively depend on the binding sites of the solvents for An(H_2O)$_1$ and An(CH_3OH)$_1$; the resultant broadening should be extensive in the spectra of the water and methanol solutions. The inhomogeneous broadening is probably responsible for the disappearance of the vibrational structures predicted for aniline in the polarizable continuum

of water and methanol (Fig. 2).

3.4. Explicit solvent molecules in the first shell

In solutions, an aniline molecule is surrounded by numerous solvent molecules. In a third step, we try to model such a situation, where we focus on the water and methanol solutions. As examined in section 3.3, each solvent molecule causes a shift of the the $S_1 \leftarrow S_0$ transition energy; the direction and magnitude of the shift depend on the location of the solvent molecule. Actual transition energies of aniline in the solutions should be determined by a balance between the blue-shifting effects of the N-bound solvents and the red-shifting effects of the H-bound and π-bound solvents. In order to evaluate the transition energies, we need to know the location and orientation of the solvent molecules surrounding aniline. For this purpose, we prefer not to add the solvent molecules one by one to the 1:1 complexes. Instead, we use MD simulations for allocating the solvent molecules around aniline all at once.

3.4.1 Modeling solvation structures by MD simulations

We run the MD simulations for 100 ps with a time step of 1.0 fs. The total energies and other quantities converge within the first 15 and 25 ps for the water and methanol solutions, respectively. Then, we use the equilibrium trajectory in the 50–100 ps range for subsequent analyses. According to a radial distribution function drawn from the equilibrium trajectory, boundary of the first solvation shell is determined to be 4.5 Å for the water solution and 5.5 Å for the methanol solution. We extract 50 snapshots from the trajectory at an interval of 1 ps. From each snapshot, we pick out the solvent molecules inside the boundary to construct a model structure with a complete solvation shell. In these model structures, the number of the solvent molecules is 31–44 for water and 30–40 for methanol. An example of the model structure is provided in Fig. 5a.

3.4.2 $S_1 \leftarrow S_0$ transition

All the molecules in the model structures are considered explicitly in TD-DFT calculations for the absorption spectra. Each model structure is placed in a cavity within the polarizable continuum. A solvent excluded surface (SES) is used instead of van der Waals (VDW) atomic radii for determining the cavity, in order to avoid unphysical double counting of solvation effects from both the explicit solvents and the dielectric continuum between explicit solvent molecules [18]. Then TD-DFT calculations are performed for predicting the vertical transition energy and the oscillator strength for the $S_1 \leftarrow S_0$ transition. The results are plotted in Fig. 6. For the model structures of the water solution, the transition energies are predicted in the 34628–37358 cm^{-1} region with an average value of 36367 cm^{-1}. The data points appear on both sides of the energy for aniline in the polarizable continuum of water (36741 cm^{-1}). As already noted, the direction of the shift is determined by a balance between the blue-shifting effects of the N-bound solvents and the red-shifting effects of the H-bound and π-bound solvents. Fig. S3a of SM shows the central region of the model structure that gives the lowest transition energy. There is no water molecule adjacent to the nitrogen atom of aniline. The distances between the nitrogen atom and the hydrogen atoms of water (i) are 2.9 and 3.0 Å and the O–H···N angles are 99° and 95°, suggesting that the O–H···N interactions are negligibly weak. Fig. S3b of SM displays the central region of the model structure that gives the highest transition energy. There are two water molecules adjacent to the nitrogen atom of aniline. For waters (ii) and (iii), the H···N distances are 2.2 and 2.6 Å and the O–H···N angles are 157° and 154°, respectively, indicating the presence of two O–H···N hydrogen bonds.

For the methanol solution, the transition energies are predicted in the 34599–37269 cm^{-1} region with an average value of 35681 cm^{-1}. Again, the data points appear on both sides of the energy for aniline in the polarizable continuum of methanol (36746 cm^{-1}). Fig. S3c of SM shows the central region of the model structure that gives the lowest transition energy. There is no methanol molecule hydrogen-bonded to the nitrogen atom of aniline. Fig. S3d of SM displays the central region of the model structure that gives the highest transition energy. The H···N distance of methanol (iv) is 1.8 Å and the O–H···N angle is

165°, indicating a strong O–H···N hydrogen bond.

The number of 50 for the model structures (or snapshots) examined is probably small for reproducing the absorption spectra [18]. Nevertheless, the differences between the highest and lowest transition energies among the 50 model structures amount to 2730 and 2669 cm^{-1} for the water and methanol solutions, respectively. The large differences suggest that the 50 model structures are sufficient for our purpose to sample various solvation environments of aniline. In this sense, the values of 2730 and 2669 cm^{-1} can be regarded as widths due to inhomogeneity in the solvation environments, which are comparable with the widths of the absorption bands observed experimentally. Meanwhile, the averaged transition energy for the water solution (36367 cm^{-1}) is larger than that for the methanol solution (35681 cm^{-1}) by 686 cm^{-1}. This result is consistent with the observation that the absorption maximum of the water solution (≈35700 cm^{-1}) is blue-shifted from that of the methanol solution (≈35150 cm^{-1}) by approximately 550 cm^{-1}. In this regard, our models with the explicit solvent molecules in the first shell are successful in reproducing the characteristic features of the experimental absorption spectra. The success encourages us to look closely at these model structures and use them for a further analysis of the aniline–solvent interactions in detail.

3.5. Solvation sites and spectral shifts

For a quantitative analysis of the aniline–solvent interactions, the number of solvent molecules is too large in the model structures used in section 3.4. Therefore, we extract the central region from the model structure to prepare the An(solvent)$_k$ cluster containing only k (≤ 7) solvent molecules in close contact with aniline. The promolecular noncovalent interaction (NCI) analysis [25] helps us know whether the interaction is significant or not between aniline and a particular solvent molecule. In the resulting An(solvent)$_k$ cluster, the solvent molecules are classified into three categories: N-bound, H-bound, and π-bound solvents. Then we construct three types of An(solvent)$_{k-l}$ sub-clusters by eliminating l solvent molecules belonging to a specified category from the An(solvent)$_k$ cluster, as

exemplified below.

We choose seven model structures, I_w–VII_w for the water solution and I_m–VII_m for the methanol solution; these model structures have the $S_1 \leftarrow S_0$ transition energies around the most probable value of each solution. Let us look at the the model structure VII_w (Fig. 5a) for aniline in water. This structure contains 36 water molecules in the first shell. Removal of distant water molecules from VII_w results in $VII_w(5)$ (Fig. 5b), which has five water molecules ($k = 5$) in close contact with aniline. We choose VII_w as an example, because the distinction among the solvation sites is rather clear in $VII_w(5)$. The molecule labelled (i) is an N-bound water, (ii) and (iii) are H-bound waters, and (iv) and (v) are π-bound waters. Elimination of the N-bound water (i) from $VII_w(5)$ yields the sub-cluster $VII_w(5–1N)$ (Fig. 5c). Elimination of the H-bound waters (ii) and (iii) results in $VII_w(5–2H)$ (Fig. 5d). Elimination of the π-bound waters (iv) and (v) gives rise to $VII_w(5–2\pi)$ (Fig. 5e). Then the vertical transition energies are calculated for the four clusters; the results are as follows: 36603 cm^{-1} for $VII_w(5)$, 35592 cm^{-1} for $VII_w(5–1N)$, 37283 cm^{-1} for $VII_w(5–2H)$, and 36957 cm^{-1} for $VII_w(5–2\pi)$. The transition energies of the $VII_w(5–1N)$, $VII_w(5–2H)$, and $VII_w(5–2\pi)$ sub-clusters are shifted by –1010, +680, and +354 cm^{-1}, respectively, from that of $VII_w(5)$. We interpret these results that the N-bound water (i) in $VII_w(5)$ has an effect of shifting the transition energy of aniline by 1010 cm^{-1} to higher energy. The same interpretation is just as valid for the H-bound and π-bound waters. In order to corroborate the analysis using the $An(solvent)_k$ cluster, we eliminate each of the N-bound, H-bond, and π-bound waters from the original model structure VII_w instead of $VII_w(5)$. The transition energies of the structures with the vacancies of –1N, –2H, and -2π are shifted by –1515, +935, and +588 cm^{-1}, respectively, from that of VII_w. Accordingly, the analysis using $VII_w(5)$ underestimates the magnitude of the shifts by 30–40 % with respect to the analysis using the original VII_w structure. We expect a similar level of accuracy for the analysis using other $An(solvent)_k$ clusters.

We conduct the analysis using the $An(solvent)_k$ cluster also for the model structures I_w–VI_w and I_m–VII_m. The results are indicated in Fig. 7 in the form of the relative transition energies (or the spectral shifts). For each of $I_w(6)$–$VII_w(5)$ (Fig. 7a), the magnitude of the

shift of the (k–1N) sub-cluster is much larger than those of the (k–lH) and (k–$l\pi$) sub-clusters. This means that the effect of a single N-bound water is larger than those of multiple H-bound and π-bound waters.

Fig. 7b shows the data for I_m–VII_m, which are different from the data for I_w–VII_w in several points. First, there is no stick corresponding to the (k–lN) sub-cluster in the rows of $I_m(3)$ and $II_m(3)$, because no N-bound methanol molecule is identified in I_m and II_m. Fig. S4a,b of SM illustrates methanol molecules only in the vicinity of the NH_2 group of aniline in I_m and II_m. In I_m (Fig. S4a), methanol (i) directs the methyl group instead of the OH group toward aniline. In II_m (Fig. S4b), methanol (ii) directs the OH group toward the nitrogen atom, but the H···N distance is large (3.5 Å) and the N–H···O angle is largely bent (102°). Second, the sticks corresponding to the (k–lN) sub-clusters appear at positive shifts for $III_m(4)$ and $VII_m(3)$. Fig. S4c of SM depicts the geometry of $III_m(4)$. The OH group of methanol (iii) points to the nitrogen atom of aniline, but the methyl group is close to the phenyl ring at the same time. In addition, the H···N distance of 2.55 Å is not small enough. Fig. S4d of SM represents the geometry of $VII_m(3)$. As in the case of methanol (iii) in $III_m(4)$, the OH group of methanol (iv) points to the nitrogen atom, but the methyl group is close to the phenyl ring at the same time. These configurations might be responsible for the exceptional behavior of the (k–lN) sub-clusters. Finally, the effect of the N-bound methanol is much less pronounced than that of the N-bound water, as the magnitude of the shifts of the (k–lN) sub-clusters is at most 554 cm^{-1}. However, it will turn out that the interaction with the N-bound methanol is not necessarily weaker than that with the N-bound water, as will be explained in section 3.6.

The analyses of the 1:1 complexes demonstrate that the N-bound solvent has an ability to largely blue-shift the transition energy. All of $I_w(6)$–$VII_w(5)$ possess such an N-bound water molecule; the effect of which is verified by the large red shift predicted for each (k–lN) sub-cluster. For the methanol solvation, on the other hand, the (k–lN) sub-clusters of only $IV_m(5)$, $V_m(7)$, and $VI_m(6)$ show moderate red shifts. Furthermore, the N-bound methanol is absent in the case of $I_m(3)$ and $II_m(3)$. It is tempting to speculate that a water

molecule is incessantly hydrogen-bonded to the nitrogen atom of aniline in the water solution, whereas the probability is much smaller for a methanol molecule to form such a hydrogen bond in the methanol solution. Fig. S5 of SM shows the distributions of the distances between the nitrogen atom of aniline and the nearest-neighbor hydroxyl hydrogen atom of water or methanol for the 50 model structures. The distribution for water has a narrower width with a maximum at the 2.0–2.5 Å bin; the distance falls within 1.5–2.5 Å for 82 % of the model structures. On the other hand, the distribution for methanol is wider with a maximum at the 3.0–3.5 Å bin; only 28 % of the model structures have the distance within the 1.5–2.5 Å range. The difference in the distributions supports the speculation made above.

Although the binding energy of the N-bound isomer of $An(CH_3OH)_1$ is larger than that of $An(H_2O)_1$, methanol molecules have a smaller probability to form an O–H···N hydrogen bond with aniline in solutions. As a result, methanol molecules have a smaller chance to exert the blue-shifting effect on the $S_1 \leftarrow S_0$ transition of aniline. We understand that, for this reason, the absorption maximum of the methanol solution (≈35150 cm^{-1}) is less blue-shifted than that of the water solution (≈35700 cm^{-1}).

3.6. Similarity and dissimilarity between water and methanol

As we all know, both water and methanol are polar and protic solvents. They have polar hydroxy group(s) and are involved in hydrogen bonding. Hydrogen-bond network structures in liquid phase have been extensively studied by various experimental and theoretical methods [26,27]. Water can be four coordinated, i.e., it accepts two hydrogen atoms from adjoining molecules while donates its two hydrogen atoms to other adjoining molecules. Accordingly, water prefers to form three-dimensional (3-D) hydrogen-bond networks [26,27]. On the other hand, methanol can be three coordinated at maximum, because the donation of two hydrogen atoms is not possible. It has been suggested that methanol molecules mainly form short linear chains or small rings in neat liquid [28–30].

The 1:1 aniline–water and aniline–methanol complexes have a lot in common, as examined in section 3.3. Three isomers are present: the N-bound, H-bound, and π-bound

isomers. For both complexes, the dissociation energy is largest for the N-bound isomers and smallest for the H-bound isomers in the S_0 state. The $S_1 \leftarrow S_0$ excitation weakens the intermolecular interactions for the N-bound isomers, while strengthens the interactions for the H-bound and π-bound isomers. As a result, the $S_1 \leftarrow S_0$ transition energies of the N-bound isomers show blue shifts, while those of the H-bound and π-bound isomers show red shifts. The magnitude of the shifts is largest for the N-bound isomers and smallest for the π-bound isomers. Regarding the effects of a single solvent molecule on the $S_1 \leftarrow S_0$ transition of aniline, water and methanol have remarkable similarities.

For aniline surrounded by a large number of solvent molecules, on the other hand, we recognize significant differences between water and methanol, as described in sections 3.4 and 3.5. At least one water molecule is almost incessantly bound to the nitrogen atom of aniline and shifts the $S_1 \leftarrow S_0$ transition to higher energy. In contrast, the probability of finding the N-bound methanol is much smaller than that of the N-bound water. In the methanol solution, the aniline molecule suffers less frequently from the blue-shifting effects of the N-bound solvent molecule.

The difference in the solvent effects can be interpreted by considering the difference in the hydrogen-bond structures of the neat liquids. Because water has two OH groups, a dangling OH group can arise from a molecule located at the surface of the 3-D networks. Such a surface water molecule with the dangling OH group can act as a donor of the O–H···N hydrogen bond with aniline. On the other hand, methanol has only a single OH group. Accordingly, only the molecule at one end of a hydrogen-bond chain can be a donor of the O–H···N hydrogen bond. Other methanol molecules must break away from hydrogen-bonded chains or rings to be the donor. Such a process is expected to be less likely than the O–H···N bond formation by a water molecule that can remain in the network. This idea can be used to explain the computational result that the N-bound methanols are less probable than the N-bound waters, although the solvent molecules in actual solutions fluctuate dynamically.

4. Conclusions

We have carried out theoretical investigations of the $S_1 \leftarrow S_0$ transition of aniline dissolved in solutions. It has been stated that, for aniline in water and methanol solutions, the O–H···N hydrogen bond should become weaker in the S_1 state, while the N–H···O hydrogen bond should be stabilized in the S_1 state [15–17]. Our calculations for the 1:1 aniline–water and aniline–methanol complexes predict that the $S_1 \leftarrow S_0$ excitation weakens the intermolecular interactions in the N-bound isomers, while strengthens the interactions in the H-bound and π-bound isomers. These predictions confirm the statement made in the previous experimental studies [15–17]. As a result of the weakening or strengthening of each hydrogen bond, the $S_1 \leftarrow S_0$ transitions of the N-bound isomers show blue shifts, while those of the H-bound and π-bound isomers show red shifts. Not only the magnitude but also the direction of the spectral shifts varies depending on the location of the solvent molecule.

Both water and methanol have polar hydroxy group(s) and are involved in hydrogen bonding with a solute molecule. Nevertheless, the maximum of the absorption spectrum of aniline in water shifts slightly to higher energy than that in methanol. For studying the solvation of aniline, it is not efficient to use gas-phase clusters, because they rarely achieve the ideal of forming a complete solvation shell around aniline. Therefore, we use MD simulations to allocate the solvent molecules around aniline all at once, instead of adding the solvent molecules one by one. TD-DFT calculations for the models of the solvation structures are successful to reproduce the observed spectral shift. Analyses by using the sub-clusters reveal that the N-bound solvent plays a central role in shifting the $S_1 \leftarrow S_0$ transition to higher energy. MD simulations suggest that at least one water molecule is almost incessantly hydrogen-bonded to the nitrogen atom of aniline in the water solution, whereas the probability is much smaller for a methanol molecule to form such a hydrogen bond in the methanol solution. Such a difference in the local solvation environment is concluded to be responsible for the observed spectral shift. The dissimilarity in the solvent effects between water and methanol is attributable to the difference in the coordination behavior; water can be double donor while methanol can only be single donor.

Acknowledgments

We thank Prof. Norio Yoshida of Nagoya University at present for helpful advice on the MD simulations. The computations are carried out by using the computer facilities at Research Institute for Information Technology, Kyushu University.

Supplementary material

Supplementary data to this article can be found online at https://...

References

[1] T.S. Zwier, The spectroscopy of solvation in hydrogen-bonded aromatic clusters, Annu. Rev. Phys. Chem. 47 (1996) 205–41. https://doi.org/10.1146/annurev.physchem.47.1.205.

[2] T. Ebata, A. Fujii, N. Mikami, Vibrational spectroscopy of small-sized hydrogen-bonded clusters and their ions, Int. Rev. Phys. Chem. 17 (1998) 331–361. https://doi.org/10.1080/014423598230081.

[3] B. Brutschy, The structure of microsolvated benzene derivatives and the role of aromatic substituents, Chem. Rev. 100 (2000) 3891–3920. https://doi.org/10.1021/cr990055n.

[4] Ch. Janzen, D. Spangenberg, W. Roth, K. Kleinermanns, Structure and vibrations of phenol$(H_2O)_{7,8}$ studied by infrared-ultraviolet and ultraviolet-ultraviolet double-resonance spectroscopy and *ab initio* theory, J. Chem. Phys. 110 (1999) 9898–9907. https://doi.org/10.1063/1.478863.

[5] K. Mizuse, T. Hamashima, A. Fujii, Infrared spectroscopy of phenol–$(H_2O)_{n>10}$: Structural strains in hydrogen bond networks of neutral water clusters, J. Phys. Chem. A 113 (2009) 12134–12141. https://doi.org/10.1021/jp9061187.

[6] I. León, P.F. Arnáiz, I. Usabiaga and J.A. Fernández, Mass resolved IR spectroscopy of aniline–water aggregates, Phys. Chem. Chem. Phys. 18 (2016) 27336–27341. https://doi.org/10.1039/C6CP04373A.

[7] T. Nakanaga, K. Kawamata, F. Ito, Infrared depletion spectroscopy of the aniline–H_2O^+ cluster cation, Chem. Phys. Lett. 279 (1997) 309–314. https://doi.org/10.1016/S0009-2614(97)01059-2.

[8] U. Spoerel, W. Stahl, The aniline–water complex. Rotational spectrum and molecular structure, J. Mol. Spectrosc. 190 (1998) 278–289. https://doi.org/10.1006/jmsp.1998.7600.

[9] G. Piani, M. Pasquini, I. López-Tocón, G. Pietraperzia, M. Becucci, E. Castellucci, The aniline–water and aniline–methanol complexes in the S_1 excited state, Chem. Phys. 330 (2006) 138–145. https://doi.org/10.1016/j.chemphys.2006.08.004.

[10] M. Haeckel, W. Stahl, The microwave spectrum and molecular structure of the hydrogen-bonded aniline–methanol complex, J. Mol. Spectrosc. 198 (1999) 263–277.

https://doi.org/10.1006/jmsp.1999.7969.

[11] S. Jiang , D.H. Levy, van der Waals complex and solvatochromism studies of substituted benzenes and naphthalenes, J. Phys. Chem. A 107 (2003) 6785–6791. https://doi.org/10.1021/jp034357b.

[12] Y. Hu, E.R. Bernstein, Photoionization and vibrational spectroscopy of the aniline–methanol clusters, J. Phys. Chem. A 113 (2009) 639–643. https://doi.org/10.1021/jp807049e.

[13] H.S. Park, S.H. Nam, J.K. Song, S.M. Park, Photoinduced ionization and dissociation of aniline–(methanol)$_n$ clusters, Int. J. Mass Spectrom. 262 (2007) 73–79. https://doi.org/10.1016/j.ijms.2006.10.006.

[14] W.F. Forbes, I.R. Leckie, Light absorption studies. part xiii. The electronic absorption spectra of ring-substituted anilines, Can. J. Chem. 36 (1958) 1371–1380. https://doi.org/10.1139/v58-202.

[15] J.C. Dearden, W.F. Forbes, The study of hydrogen bonding and related phenomena by ultraviolet light absorption: part iv. Intermolecular hydrogen bonding in anilines and phenols, Can. J. Chem. 38 (1960) 896–910. https://doi.org/10.1139/v60-127.

[16] G. Perichet, R. Chapelon, B. Pouyet, Emission and intersystem crossing quantum yields of aniline solutions: photostationary state diagram, J. Photochem. 13 (1980) 67–74. https://doi.org/10.1016/0047-2670(80)85060-X.

[17] G. Köhler, Solvent effects on the fluorescence properties of anilines, J. Photochem. 38 (1987) 217–238. https://doi.org/10.1016/0047-2670(87)87019-3.

[18] T.J. Zuehlsdorff, C.M. Isborn, Modeling absorption spectra of molecules in solution, Int. J. Quantum Chem. 119 (2019) e25719. https://doi.org/10.1002/qua.25719.

[19] Š. Budzák, T. Jaunet-Lahary, A.D. Laurent, C. Laurence, M. Medved', D. Jacquemin, Exploring the solvatochromism of betaine 30 with ab initio tools: From accurate gas-phase calculations to implicit and explicit solvation models, Chem. Eur. J. 23 (2017) 4108–4119. https://doi.org/10.1002/chem.201604619.

[20] F. Bettanin, S. Jurinovich, S. Caprasecca, B. Mennucci, P, Homem-de-Mello, A quantum chemical investigation of the solvatochromism of a phthalocyanine within a lipid bilayer:

Comparison between *continuum* and atomistic models, J. Photochem. Photobiol. A 344 (2017) 42–48. https://doi.org/10.1016/j.jphotochem.2017.04.033.

[21] S. Skoko, M. Ambrosetti, T. Giovannini, C. Cappelli, Simulating absorption spectra of flavonoids in aqueous solution: A polarizable QM/MM study, Molecules 25 (2020) 5853. https://doi.org/10.3390/molecules25245853.

[22] M.J. Frisch, G.W. Trucks, H.B. Schlegel et al., GAUSSIAN 16, Revision A.03, Gaussian Inc., Wallingford CT, 2016.

[23] D.A. Case, I.Y. Ben-Shalom, S.R. Brozell et al., AMBER 2018, University of California, San Francisco, 2018.

[24] H. Keller-Rudek, G.K. Moortgat, R. Sander, R. Sörensen, The MPI-Mainz UV/VIS spectral atlas of gaseous molecules of atmospheric interest, Earth Syst. Sci. Data 5 (2013) 365–373. https://doi.org/10.5194/essd-5-365-2013.

[25] E.R. Johnson., S. Keinan, P. Mori-Sánchez, J. Contreras-García, A.J. Cohen, W. Yang, Revealing noncovalent interactions, J. Am. Chem. Soc. 132 (2010) 6498–6506. https://doi.org/10.1021/ja100936w.

[26] D. Eisenberg, W. Kauzmann, The Structure and Properties of Water, Oxford University Press, New York, 1969.

[27] F. Franks (Ed.), The Physics and Physical Chemistry of Water, Vol. 1, Plenum Press, New York, 1972.

[28] T. Yamaguchi, K. Hidaka, A.K. Soper, The structure of liquid methanol revisited: a neutron diffraction experiment at –80 °C and +25 °C, Mol. Phys. 96 (1999) 1159–1168. https://doi.org/10.1080/00268979909483060.

[29] J.W. Handgraaf, E.J. Meijer, M.P. Gaigeot, Density-functional theory-based molecular simulation study of liquid methanol, J. Chem. Phys. 121 (2004) 10111–10119. https://doi.org/10.1063/1.1809595.

[30] T. Kobayashi, R. Shishido, K. Mizuse, A. Fujii, J.-L. Kuo, Structures of hydrogen bond networks formed by a few tens of methanol molecules in the gas phase: size-selective infrared spectroscopy of neutral and protonated methanol clusters, Phys. Chem. Chem. Phys. 15

(2013) 9523–9530. https://doi.org/10.1039/C3CP50985K.

Figure Captions

Fig. 1. Ultraviolet absorption spectra of aniline dissolved in cyclohexane (c-C_6H_{12}), methanol (CH_3OH), and water (H_2O) at ambient temperature. The concentration of aniline is 1.0×10^{-3} mol dm^{-3}. The spectra are recorded with a spectrophotometer (Shimadzu UV-2500PC) at a step of 0.5 nm, which corresponds to 50–75 cm^{-1} in this region.

Fig. 2. Vibronic spectra calculated for the $S_1\leftarrow S_0$ transition of aniline in the polarizable continuum of cyclohexane (c-C_6H_{12}), methanol (CH_3OH), and water (H_2O). Theoretical line spectra are convoluted with a width of 175 cm^{-1} (cf. section A.2 of SM). Vertical bars indicate the positions and relative intensities of the 0–0 transitions in three solvents.

Fig. 3. Structures of (a–c) An$(H_2O)_1$ in the S_0 state, (d, e) An$(H_2O)_1$ in the S_1 state, (f–h) An$(CH_3OH)_1$ in the S_0 state, and (i, j) An$(CH_3OH)_1$ in the S_1 state, optimized in the polarizable continuum of the respective solvents at the M06-2X(GD3)/6-311++G(d,p) level.

Fig. 4. Energies calculated for (a–e) the 0–0 transitions and (f–j) the vertical transitions of (a, f) aniline in vacuum, (b, g) aniline in the polarizable continuum, and (c–e, h–j) 1:1 aniline–solvent complexes. The height of sticks in (f–j) is proportional to the oscillator strength. Labels I–IV stand for the four isomers of An(c-C_6H_{12})$_1$ (cf. Fig. S8 of SM). N, H, and π indicate the N-bound, H-bound, and π-bound isomers, respectively.

Fig. 5. (a) Model structure VII$_w$ for aniline with 36 water molecules in the first shell. (b) An$(H_2O)_{k=5}$ cluster VII$_w$(5) formed by removing distant water molecules from VII$_w$. (c) Sub-cluster VII$_w$(5–1N) formed by eliminating the N-bound water (i) from VII$_w$(5). (d) VII$_w$(5–2H) formed by eliminating the two H-bound waters (ii and iii). (e) VII$_w$(5–2π) formed by eliminating the two π-bound waters (iv and v).

Fig. 6. Vertical transition energies (in units of cm^{-1}) and oscillator strengths of the $S_1 \leftarrow S_0$ transition calculated for the 50 model structures: aniline in water (○) and in methanol (●). Also shown are the data for aniline in the polarizable continuum of water (+) and methanol (×). Vertical bars indicate the values of the averaged transition energies of the 50 model structures for aniline in water (right) and in methanol (left). Broken curves are the experimental absorption spectra reproduced from Fig. 1.

Fig. 7. Vertical transition energies of (k–lN), (k–lH), and (k–$l\pi$) sub-clusters relative to that of An(solvent)$_k$ (stick at the origin): (a) $I_w(6)$–$VII_w(5)$ for the water solution and (b) $I_m(3)$–$VII_m(3)$ for the methanol solution. The height of sticks is proportional to the oscillator strength. For $V_m(7)$ and $VI_m(6)$, the sum of three l values is not equal to k, because a single methanol molecule occasionally binds to two different sites simultaneously.

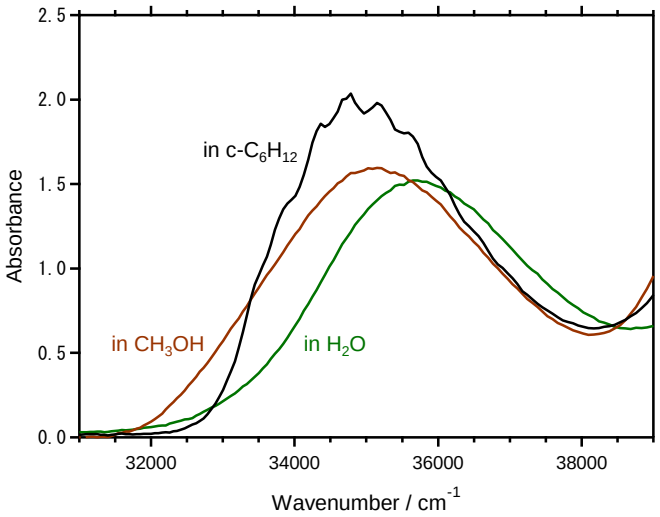

Fig. 1 Watanabe et al.

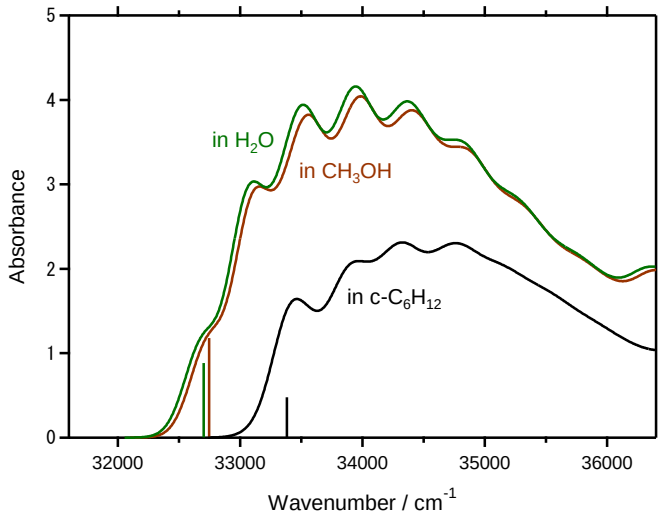

Fig. 2 Watanabe et al.

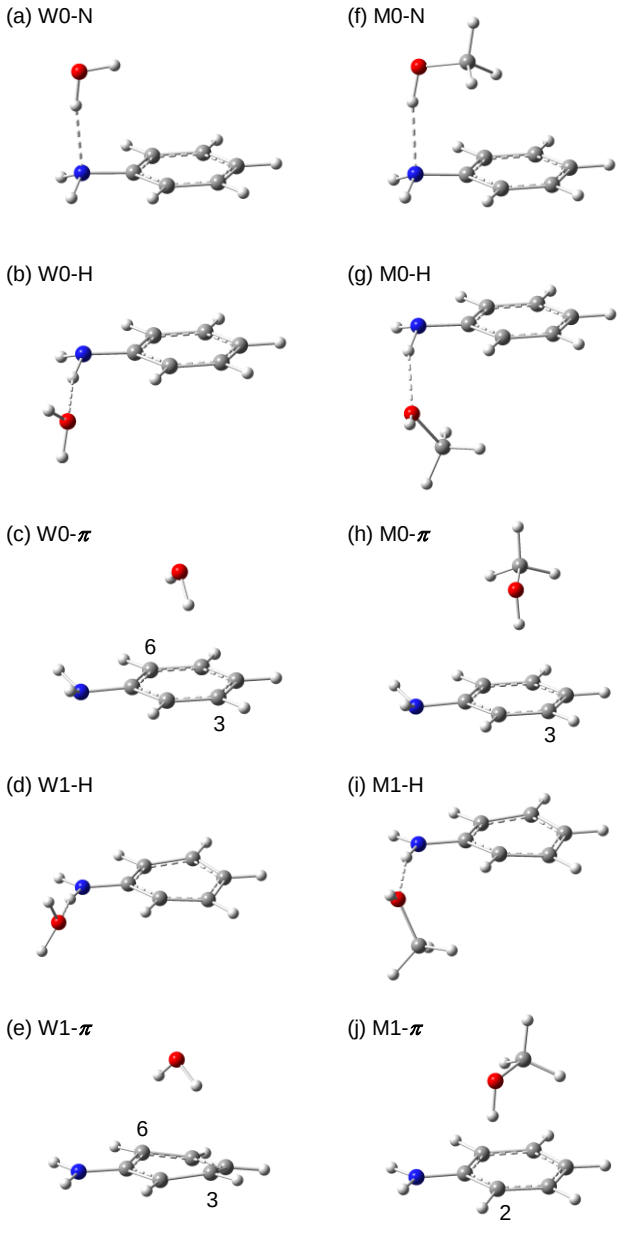

Fig. 3 Watanabe et al.

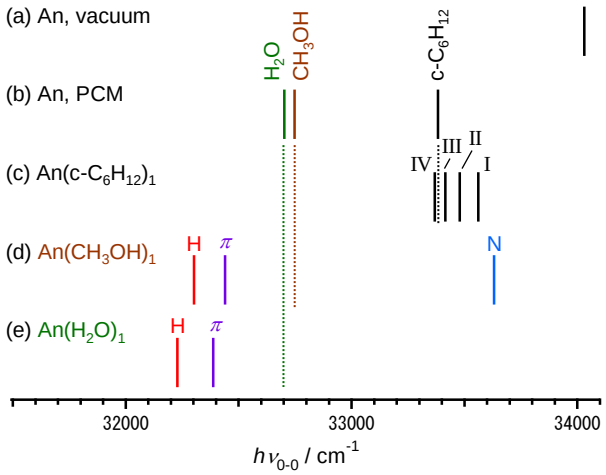

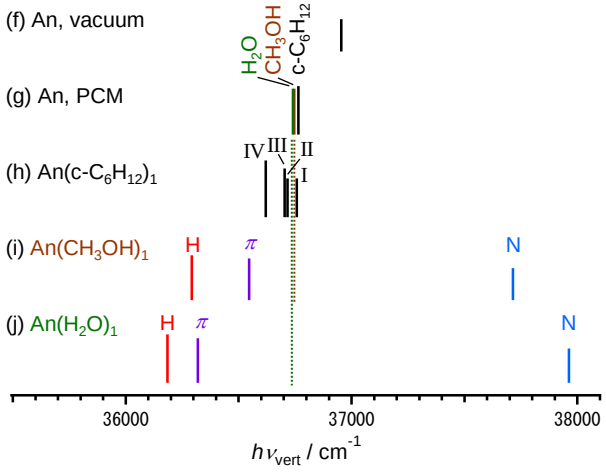

Fig. 4 Watanabe et al.

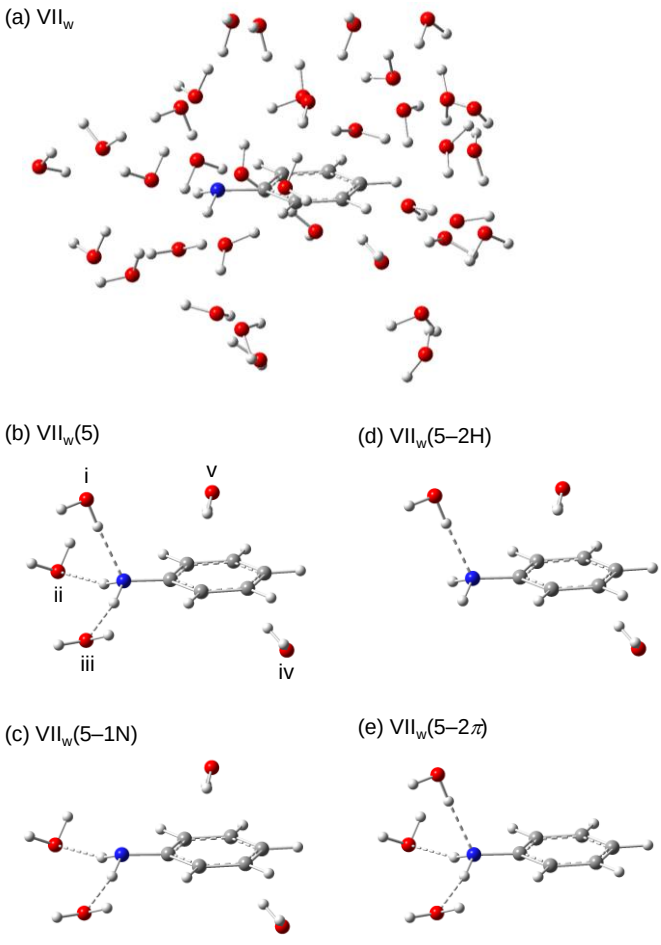

Fig. 5 Watanabe et al.

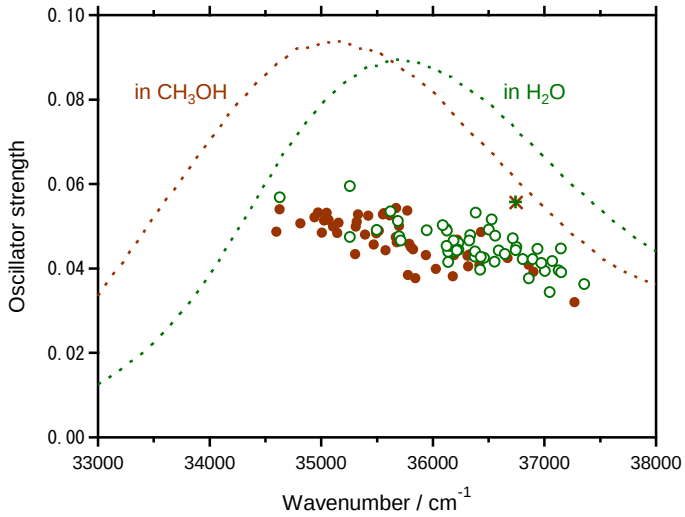

Fig. 6 Watanabe et al.

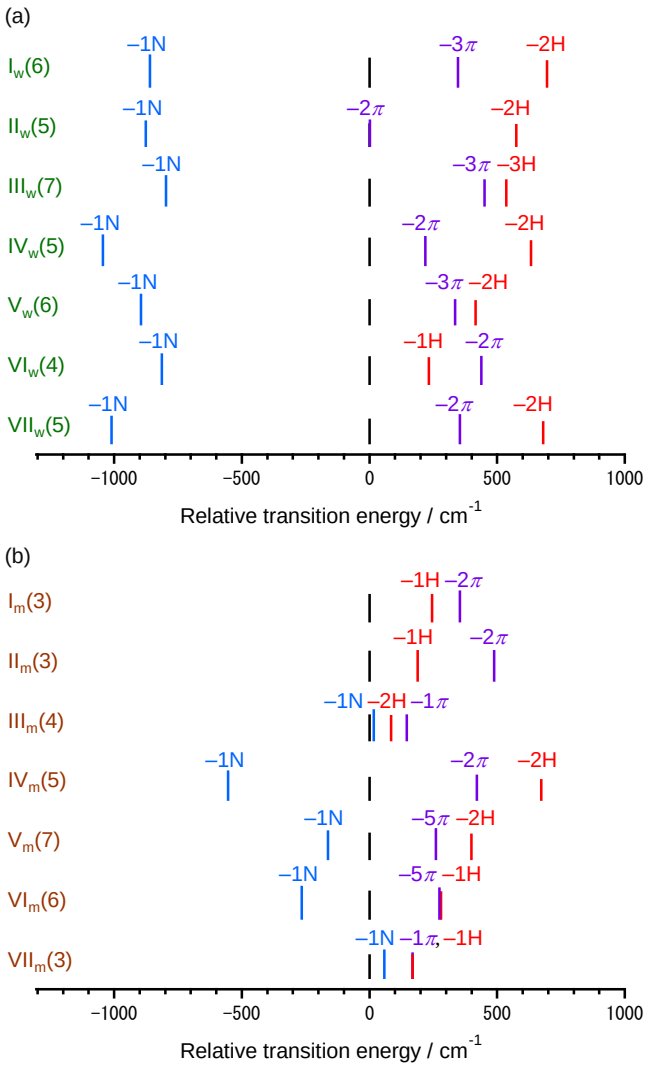

Fig. 7 Watanabe et al.